FYS-3931

Master Thesis in Space Physics

Na lidar measurements during the ECOMA/Geminids campaign with focus on Na peak density and temperature

Author:
Jørgen Østerpart

Supervisor:
Prof. Ulf-Peter Hoppe

February, 2011

FACULTY OF SCIENCE AND TECHNOLOGY

Department of Physics and Technology

University of Tromsø

Introduction

Using a resonance lidar, atomic Na (sodium) can be observed in the 80-110 km altitude range of the atmosphere. Na belongs to the alkali metal group and is highly reactive, so one could expect that it would quickly react with other particles and leave its atomic state. Its actual behaviour however includes the formation of relatively dense layers which, from the perspective of a stationary lidar, form suddenly and can last for several hours before quickly disappearing again. Several theories on the formation of these layers have been developed, including temperature dependent chemical processes, but none of them seem to explain all of the observed events.

In 2008, two articles about these sudden sodium layers were published by scientists who have worked with the Weber Na lidar at the Arctic Lidar Observatory for Middle Atmosphere Research (ALOMAR), located at Andøya, Norway ($69°16'N, 16°00'E$). Nesse et al. (2008) describe one particular Na layer observed 5 November 2005 and consider in turn how the most probable theories match the observed data during this event. Heinrich et al. (2008) identify all the sudden Na layers that have been observed on ALOMAR between August 2000 and June 2006 and investigate in particular how these coincide with sporadic E-layers (thin layers of several types of metallic ions).

The fourth ECOMA (Existence and Charged State of Meteoric Smoke Particles in the Middle Atmosphere) rocket campaign took place at the Andøya Rocket Range during November and December 2010. The Na lidar was operated to the extent possible during this period, resulting in near real-time data for two of the three rocket launches and a total of 48 hours of measurements which are presented in this text. Using the two formerly mentioned articles as a starting point, I have studied available theory about sudden Na layers and the ALOMAR Na lidar in particular, and the upper atmosphere and resonance lidars in general. While we did not observe any sudden Na layers during the ECOMA measurements, I look into an older dataset as an example.

Contents

1 The ALOMAR Na lidar

1.1 The atmosphere at 80-110 km

The focus of this thesis is a layer of neutral Na between roughly 80 and 110 km altitude, particulary the observations made with the ALOMAR Na lidar during the ECOMA 2010 rocket campaign. This section describes the characteristics of this altitude interval as well as some of the other phenomena that occur there.

Temperature: Prölss (2004) describes how the lower end of the interval has very low temperatures, as the mesopause is normally found at 80-90 km. The mean temperature there is around 160 K, although observations as cold as 120 K have been made under extreme circumstances. The mesopause temperatures are generally coldest during summer, and ice particle related phenomena such as polar mesospheric summer echoes in radar measurements and noctilucent clouds are commonly observed. In the upper part of the interval, which is the lower part of the thermosphere, temperature increases quickly to a typical value of around 300 K at 110 km. This increase of temperature is explained with absorbance of ultraviolet radiation with $\lambda < 242nm$ and an absence of efficient heat loss processes.

Constituents of the atmosphere and density: Up to about 100 km, the relative proportions of the different gases that make up the atmosphere, are well mixed due to turbulence: 78% N_2, 21% O_2, 1% argon, and trace gases. This part of the atmosphere is called the homosphere, and its upper boundary is the homopause. Homopause height varies from day to day, and sometimes hour by hour, between 80 and 120 km. The atmosphere is considered to end at the exobase, the limit where atmospheric particles are no longer gravitationally bound to the Earth. The exobase height varies between about 350 and 700 km, depending on temperature and solar activity. Between the homopause and exobase, which is within the heterosphere, gravitational settling dominates turbulence, and the proportion of heavier gases decreases while lighter gases such as N_2, O and He alternate to be the main constituent. As the 80-110 km altitude range includes the transition from the homosphere to the heterosphere, we see roughly the same mix of gases as on the surface, except that the relative O_2 density decreases in the upper parts of this interval. Atmospheric pressure and number density are of an order of around 10^{-6} at 100 km altitude compared to at the surface, and the free mean path

is about 0.1 m.

Other phenomena: Aurorae have a lower boundary of about 100 km, where the most energetic auroral electrons (around 10 eV) can react with atmospheric particles, which might be an important factor in the creation of Na layers and E-layers, as described in section 3.3. Meteors entering the atmosphere largely ablate in this altitude range and act as source for metals such as sodium, iron and magnesium (Clemesha, 1995). Because of this, we also find layers of metals other than sodium here, such as iron.

1.2 The sodium atom

Sodium has atomic number 11 and belongs in the alkali metal group, which are highly reactive. Although it makes up about 2.6% of the Earth's crust, making it the 4th most abundant element (playing an important role in living organisms), it is rarely found in its elemental form except at mid to high altitudes in the atmosphere. Sodium has thirteen recognized isotopes, of which only ^{23}Na is stable. There are two radioactive isotopes, ^{22}Na (half-life 2.6 years) and ^{24}Na (half-life 15 hours), while all remaining isotopes have a half-life of less than one minute.

The sodium atom has three electron shells, from the innermost to the outermost containing two, eight and one electron, respectively. According to quantum mechanical theory, the energy transitions of the outermost electron allow the sodium atom to absorb and re-emit photons of a finite number of discrete wavelengths, due to the finite number of possible energy states it can exist in. There are two forms of emission: Stimulated and spontanous emission. Stimulated emission can occur if a photon passes closely by an excited atom, and the energy of the photon matches one of the atom's possible energy transitions. The emitted photon is identical to the stimulating photon and travels in the same direction. Spontanous emission from excited sodium atoms happen without the presence of another photon and in a random direction, which means that if one illuminates sodium atoms in the atmosphere with a laser beam from a location on the ground, a small fraction of the emitted photons have such a direction that they reach the ground at that same location. This mechanism allows measurements with groundbased lidars.

Due to Doppler broadening, groups of these discrete energy transitions form resonance lines with finite bandwidths. For temperatures below 456 K

the D_2 line has two distinct peaks (Gibson et al., 1979), which are due to the D_{2a} and D_{2b} fine structure lines. Each of these consists of three hyperfine structure lines, which correspond to possible energy transitions between the $^2S_{3/2}$ ground state and the $^2P_{3/2}$ excited state, as shown in figure 1.

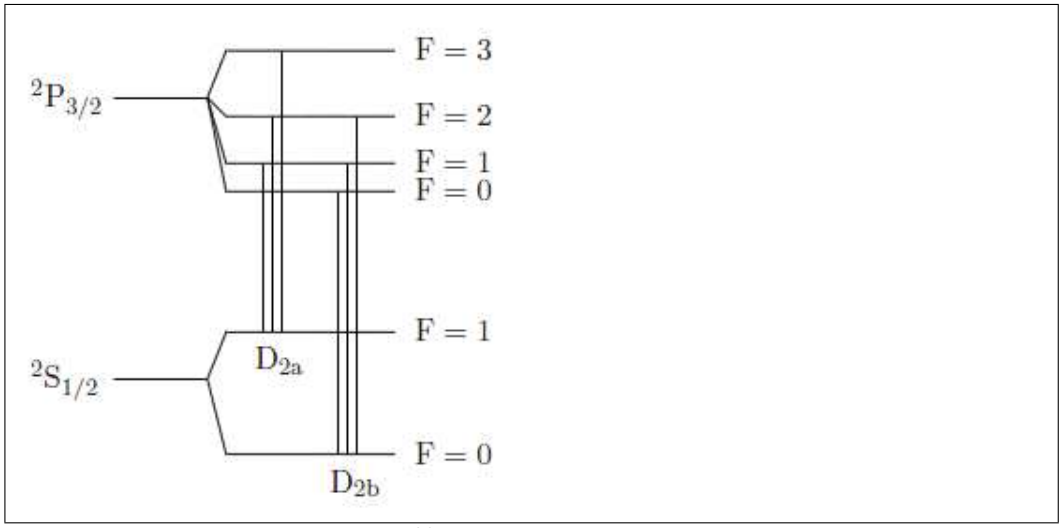

Figure 1: Energy levels of ^{23}Na connected by the D_2 resonance line hyper fine structure multiplet. The separation of levels is not drawn to scale. (Kaifler, 2009 (figure 2.3); Fricke and von Zahn, 1985 (figure 1))

1.3 Measurement principle

Sandford and Gibson (1970) describe how one can use a laser tuned to the frequency of a sodium D resonance line to measure sodium abundance in the sodium layer. Signal from up to around 35 km altitude is due to Rayleigh scattering by O_2 and N_2, while signal from around 90 km is due to scattering by atomic sodium. Note that Rayleigh signal up to about 35 km is typical for a Na lidar, while other lidars can get such a signal up to other altitudes. The signal from about 30 km altitude combined with density data from the European Centre for Medium-Range Weather Forecasts (ECMWF), is used to calibrate the instrument to properly calculate the density of sodium in the sodium layer. The linewidth of the lasers used at the time was comparable to the width of the D lines. When the available technology allowed lasers with linewidths much smaller than the D lines, it became possible to also measure temperature by estimating the shape of the D_2 line and fitting a theoretical shape to the estimated shape. This theoretical shape would correspond to a temperature (Gibson et al., 1979). The line shape was estimated by tuning

the laser to a set amount of different frequencies spread over the line and comparing the measured sodium densities. Other groups such as Fricke and von Zahn (1985), later improved these techniques.

She et al. (1992) developed the Na lidar system, which is amongst other locations in use at the Arctic Lidar Observatory for Middle Atmosphere Research (ALOMAR), located at Andøya, Norway ($69°16'N, 16°00'E$). With improved linewidth and frequency of the laser, compared to the systems mentioned above, it is possible to estimate the shape of the D_2 line by using three frequencies centered around the D_{2a} hyperfine line, as well as measure wind speed along the beam path due to the Doppler shift of the line.

Given an atmospheric volume in the sodium layer, the three frequencies are used to estimate the absorbance spectrum of the volume, which in turn is used to calculate temperature, wind speed along the beam path and sodium density (when calibrated by the Rayleigh signal at some set altitude around 30 km). The center frequency is at the center of the D_{2a} hyperfine line because this is the maximum of the D_2 resonance line, which means photons at this frequency have the same energy as the most frequent energy transitions in a sodium atom, as illustrated in figure 2. The other two frequences are $\pm 630 MHz$ from the center frequency.

Photons with the same frequency can cause different energy transitions in sodium atoms, depending on the velocity of the atoms along the beam path (the Doppler effect). Additionally, excited atoms of the same energy level can emit photons of different frequencies if they have multiple lower energy levels to transition to; for example: Atoms of the $^2P_{3/2}$, F = 1, 2 states (see figure 1), can transition to both $^2S_{3/2}$ ground states, resulting in photons with different frequencies being emitted. However, for measurements during darkness, the receiver has a bandwidth wide enough to cover all emitted frequencies, so we can basically assume that a given amount of received photons (regardless of actual frequency) corresponds to a given amount of absorbed photons. When measuring in daylight, the receiver is protected by a Faraday Anomaly Dispersion Optical Filter (FADOF) which does not have a wide enough bandwidth for this assumption, and the analysis process becomes more complex (Heinrich, 2007).

When we have measured at the three frequencies, as illustrated by the vertical bars in figure 3, we can estimate the temperature by comparing the relative signals at each frequency. If there is a large difference between the center frequency and the two shifted frequencies, it means the spectrum is

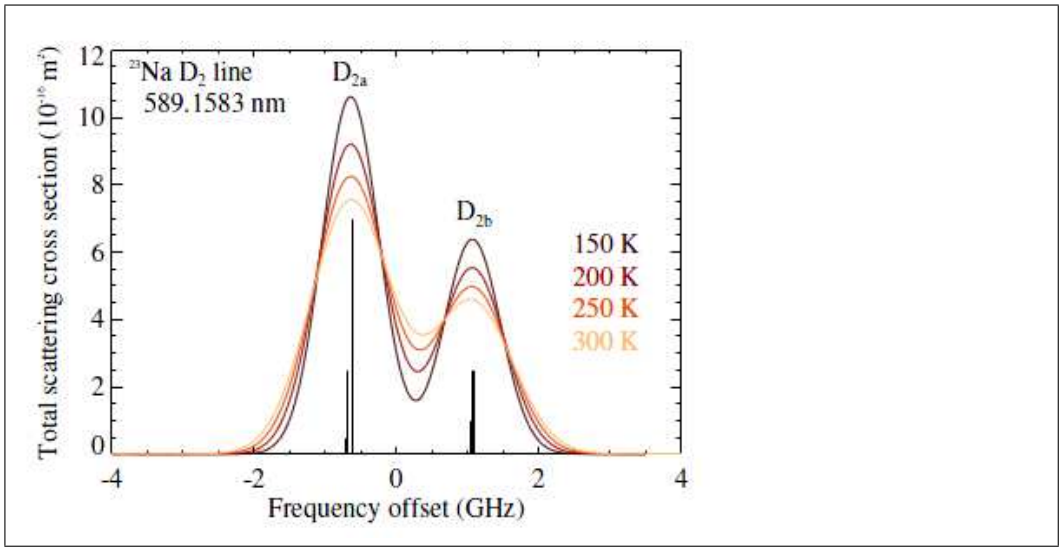

Figure 2: Variation of the scattering cross section in the Doppler broadened hyperfine structure of the ^{23}Na D_2 resonance transition for different temperatures. The relative strength of the individual lines is given by vertical bars. (Kaifler, 2009, figure 2.4)

narrow as in the left panel of figure 3, that the Doppler broadening is weak, and the temperature is low. If the difference is small, the spectrum is wider and lower as in the middle panel of figure 3, and the temperature is higher. Further, a large difference in signal strength at the two shifted frequencies, indicate a wind along the beam path, as illustrated in the right panel of figure 3. This is due to a Doppler shift of the entire spectrum.

1.4 The Na lidar system

It should be noted that the lidar is under continuous development, and the numbers and methods I present here represent the system during my measurement period in November/December 2010.

The ALOMAR Na lidar consists of the following subsystems: Seeding lasers, frequency stabilizer, acousto-optic modulator (AOM), pulsed dye amplifier (PDA) which is pumped by a pulsed YAG laser, telescopes and receiver electronics. In this text I refer to the telescopes and receiver electronics as the receiver, while the remaining subsystems make up the transmitter, which is sketched in figure 4. The seeding beam is created by using two infrared lasers

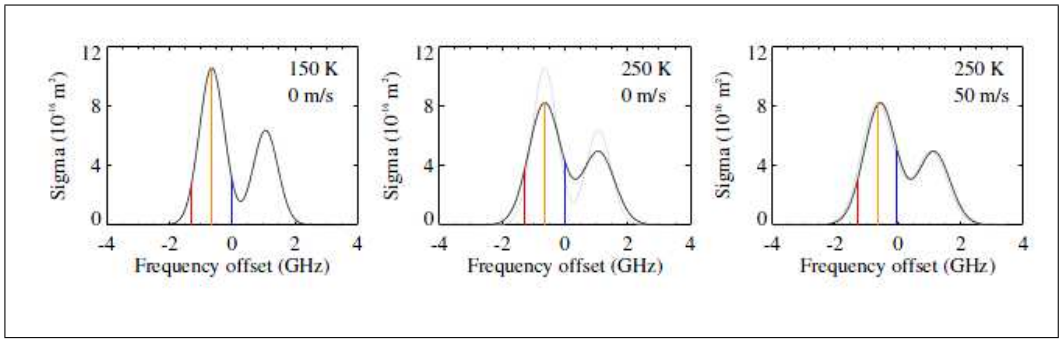

Figure 3: Variation of the total scattering cross section in the hyperfine structure of the Na D_2 resonance transition for three different atmospheric conditions. The emitted laser frequencies are marked with vertical bars. (Kaifler, 2009, figure 2.5)

that produce about 900 mW 1064 nm and 400 mW 1319 nm radiation, and a periodically poled lithium-niobate (PPLN) crystal which performs sum-frequency generation through nonlinear processes. The laser beams follow the same path into the crystal which emits a beam of around 35 mW 589 nm light (a dark yellow), along with the remaining infrared radiation, which is of no further use. A small fraction of the seeding beam is sent into a Doppler-free Na cell kept at a temperature of $78°C$, where a photomultiplier tube provides input to a computer program that locks the wavelength of the seeder beam to the D_{2a} peak. The principle behind the Doppler-free Na cell is described towards the end of this subsection. The seeding beam then passes through the acousto-optic modulator which during operation alternates between letting the beam through unchanged, changing the frequency up 630 MHZ and down 630 MHz. This step is crucial for the measurement principle, as described in subsection 1.3. The lidar transmits for 5 s at each frequency, creating data files of 15 s. Behind the acousto-optic modulator, the seeder beam normally has a power of 5-20 mW (the shifted frequencies are generally weaker than the unshifted one). In order to get sufficient photons per pulse to get a good signal from the Na layer, the seeder beam is amplified by a pulsed dye amplifier (PDA). The PDA contains an organic dye as laser medium and is pumped by a 17 W yttrium aluminium garnet (YAG) laser. This amplifies the seeding beam to 400-1000 mW in 7 ns pulses at 50 Hz. This can be split into two beams for measurements in two directions, which is standard during darkness. The receiver uses one 1.7 m telescope per beam, which feed the received photons to a photon counter through optical fibres and a series of filters to reduce background noise and protect the counter.

Finding the D_{2a} peak is done by using a Doppler-free Na cell with a

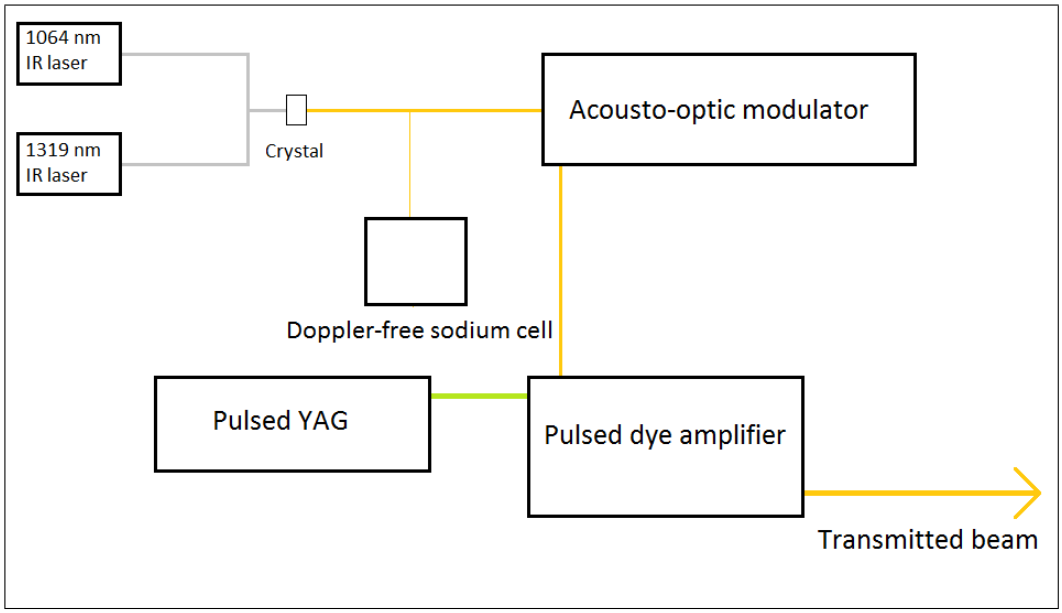

Figure 4: Conceptual sketch of the Na lidar transmitter. The size of the subsystems are not to scale.

photomultiplier tube (PMT) connected to a computer (She et al., 1992). The computer can tune the wavelength of one of the infrared lasers, and by extension the wavelength of the seeder beam. A small fraction of the seeding beam, which initially has a wavelength close to the D_{2a} line, is sent through a cell containing Na gas at a temperature of $78°C$, reflects on a mirror and goes back through the cell precisely along the same path. If the wavelength is off the D_{2a} peak, the beam excites Na atoms that have a certain velocity along the beam path, due to the Doppler effect. Since the beam is reflected on the back mirror, and goes through the gas in both directions, it excites atoms that are moving in both directions. This creates a glow which is registered by the PMT. If the frequency is exactly on the D_{2a} peak, the beam will excite atoms that are at rest, during both passes through the cell. This means there is a higher degree of saturation if the frequency is at the D_{2a} peak, which is evident in a reduced gas glow. This allows a computer program, which is fed input from the PMT, to lock on to the minimum at the D_{2a} peak frequency and tune the seeder laser to stay close to it during operation.

2 ECOMA/Geminids rocket campaign

In the period 2006-2010, four ECOMA (Existence and Charged State of Meteoric Smoke Particles in the Middle Atmosphere) rocket campaigns took place on Andøya Rocket Range. The fourth was performed from November 25th to December 20th 2010 and included three sounding rocket launches, during which the ALOMAR Na lidar was operated to the extent possible. The goal of ECOMA/Geminids was to study the effect of meteor showers on the meteoric smoke particle density, by making in situ measurements before, during and after the Geminids meteor shower. During a sounding rocket launch, it is of great benefit to make simultanous measurements with as many other instruments as possible. If these instruments measure different atmospheric variables than the rocket payload does, one can gain more understanding of the ongoing processes and phenomena, while if several instruments measure the same variable, one can get more accurate data. Some instruments allow real-time monitoring of atmospheric conditions, giving scientists more information when deciding when to launch the rocket. The ALOMAR Na lidar measures Na density, temperature and wind speeds in the 80-110 km altitude range, and it can provide nearly real-time data. Additionally, because meteors are the likely source of Na in the atmosphere, making measurements during a meteor shower is potentially extra interesting.

The campaign was a scientific success, as at least four abstracts have been submitted for the 20th ESA Symposium on European Rocket & Balloon Programmes and Related Research, which will be held in 22-26 May 2011. Further results and publications are likely after the data have been analysed in more detail. Some of these publications will include data from the Na lidar.

2.1 The Geminids

The Geminids are a meteor storm in mid-December, with a peak on the 14th of the month. It is caused by 3200 Phaethon, a near-Earth asteroid with a diameter of about 5.1 km. It shares some characteristics with comets, and its perihelion is only 0.14 AU, which is closer to the Sun than any other known asteroid (because of this it is named after Phaëton, the son of the Greek Sun god, Helios). The Geminids have gotten their name because the

Earth's velocity vector points towards the constellation Gemini (Tvillingene in Norwegian) during its peak, causing a large portion of the meteors to apparently come from this area of the sky. Meteors from the Geminids have a typical velocity of 36 km/s with respect to the Earth's atmosphere. They were first observed in the late 1800s, as a weak and not particularly interesting meteor shower, but have gradually increased in strength since.

2.2 ECOMA 1-6 (2006-2008)

The first ECOMA campaign included two sounding rocket launches in September 2006. The main goal was to measure the distribution of meteoric smoke particles and make background ionosphere measurements. The second and third campaigns took place during summer in 2007 and 2008, with focus on the relationship between meteoric smoke particles and the ice-related phenomena noctilucent clouds and polar mesospheric summer echoes.

2.3 Results from the ALOMAR Na lidar during ECOMA 7-9 (2010)

ECOMA 7-9 were launched in December 2010, before, during and after the peak of the Geminids meteor shower (see table 2.3). We were able to make measurements with the Na lidar during the second and third launch, but not the first because of a thick cloud layer. Additionally, other measurements were made in the campaign period, between 25 November and 20 December. All usable Na density, windspeed and temperature data are presented here chronologically, with emphasis on the rocket launches and any sudden changes in density or temperature.

Rocket	Time of launch (UT)
ECOMA 7	4:21 on 4 December 2010
ECOMA 8	3:24 on 13 December 2010
ECOMA 9	2:36 on 19 December 2010

Table 1: Times of launch for three sounding rockets during the ECOMA 2010 campaign.

All of these measurements were made with two beams, as is standard when measuring in darkness. For most of the time, both beams had a 20° angle from zenith, while beam 1 was pointed towards north (azimuth 0°) and beam 2 was pointed towards east (azimuth 90°). The 20° angle from zenith means that atmospheric volumes from which we have collected data at different altitudes, also are separated by a horizontal distance. For example, data from 85 and 100 km altitude stem from atmospheric volumes which are about 5.5 km apart horizontally. Thus one of the underlying assumptions we make when analysing lidar data, is that the atmospheric conditions do not vary significantly over horizontal differences of this magnitude. The atmospheric volumes seen by beam 1 and beam 2 are about 42 km apart at 80 km altitude, 49 km apart at 95 km and 57 km apart at 110 km, with the beam 1 volume being located to the northwest in relation to the beam 2 volume.

The raw data from the Na lidar consists of data files containing 15 seconds of measurements (five seconds for each wavelength, as described in section 1.3). When analyzing the data, one integrates a number of these files depending on desired temporal resolution and statistical certainty. Usually, one encounters a trade-off between these two desirables. In this analysis, I have chosen to set a maximum uncertainty in the variables: The Na density plots have a maximum uncertainty of $100 \cdot 10^6/m^3$, the temperature plots $5K$ and the windspeed plots $5m/s$. Data points that do not fulfill these uncertainty criteria are not plotted. The absolute temperatures are at this time preliminary and will require more work, but the relative temperatures are already correct within the above mentioned uncertainty.

When processing the data, I have integrated over two minutes for the Na density and temperature data, and 15 minutes for the windspeed data, to create height profiles for each variable. The data are presented in colour plots, as well as individual profiles for the same time as the launch of ECOMA 8 and 9. The colour plots are smoothed over two adjacent bins, and the display interval for the measured variables is chosen for each dataset so that atmospheric structures are easily visible. The altitude interval is fixed to 80-110 km for easy comparison. I have used the colour plots to identify these structures and drawn values from the individual height profiles where I have studied them closer.

The structures I have focused on, are short-scale (up to around 30 minutes) changes in Na density and temperature. Section 3.2 describes one of the theories concerning temperature dependent chemical processes involving

Na. The key result in this theory is that increased temperature is likely to cause an increased Na abundance. A simplified formula is that a temperature increase of 10 K can lead to a doubling of Na abundance. However, temperature is not the only phenomenon that can affect Na density. Gravity waves are very commonly seen in atmospheric measurements of horizontal layers such as the Na layer (Hoppe, 89). Gravity waves can occur if the atmosphere is stably stratified so that if an atmospheric fluid parcel is displaced, it will undergo buoyancy oscillations (Holton, 2004). Gravity waves are a complex topic, with several classes of waves (such as acousto-gravity or inertio-gravity waves) with a wide range of wavelengths and frequencies (Fritts and Alexander, 2003). The vertical component of a gravity wave wind oscillation can significantly affect the shape of the Na layer. An upwards wind causes an increase of Na density above the layer maximum, while it causes a decrease below the maximum. Additionally, the upwards wind causes adiabatic expansion in the rising fluid parcel, which decreases the density above the maximum, counteracting the former effect. A downwards wind has an inverse effect. This means a gravity wave affects a Na layer more strongly below the layer maximum.

Gravity waves also cause temperature oscillations, and if they occur alongside the wind effects described above, we could expect to some degree that a near simultaneous change in Na density and temperature might both be due to a propagating gravity wave, rather than the Na density change being due to the temperature change. Because of this, I am cautious not to assume any direct cause-effect relationship between such structures in the Na lidar data, but rather note whether Na density changes are accompanied by temperature changes. Partly because of this process, I measure Na density and temperature changes at the altitude of the Na density peak. I have estimated the development of Na density and temperature at the peak altitude throughout the measurements, by reading the data from 15 minute integration height profiles. Additionally, I have plotted the peak altitude as function of time, as well as the altitude where the Na density is half of the peak value. These data will be used to calculate a typical shape of the Na layer for the measurements made during ECOMA/Geminids.

26 November

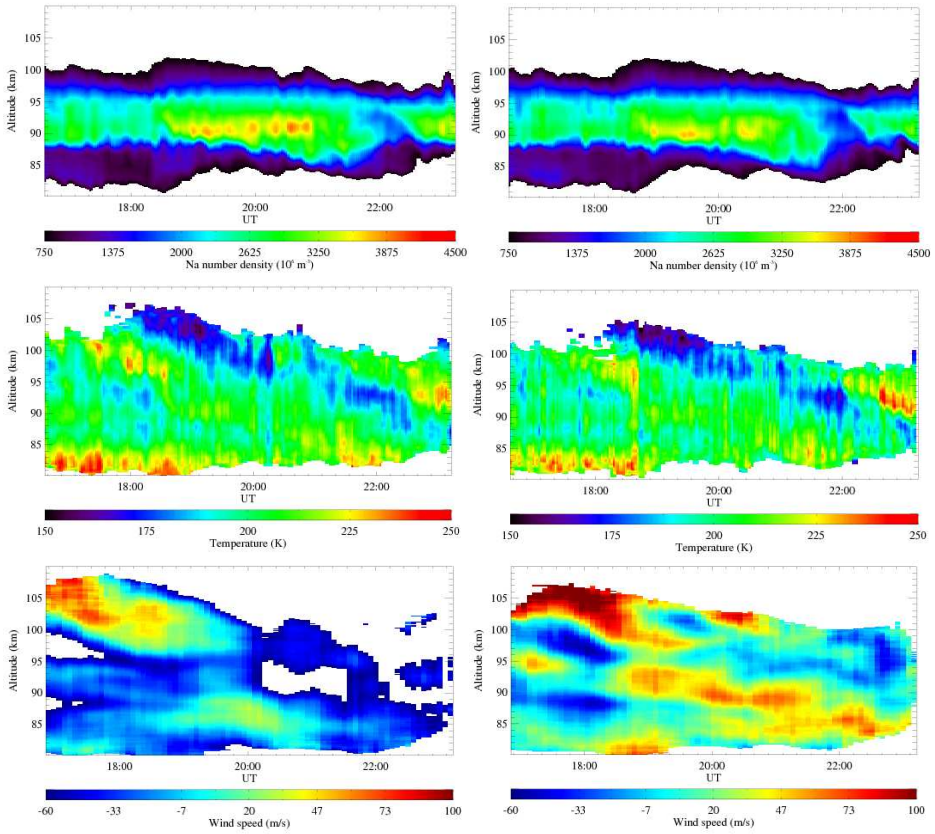

Figure 5: Na density (top), prelim. temperature (middle) and windspeed data (bottom) for 26 November 2010. Left row is from beam 1 (north), right row is from beam 2 (east).

The 26 November dataset includes several interesting phenomena. The Na density and temperature data from the two beams are remarkably similar and show almost the same atmospheric structures, with beam 2 apparently lagging 5-10 minutes behind beam 1. This can be explained by looking at the windspeed data: As mentioned in the previous subsection, the atmospheric volume observed by beam 1 is located about 42-57 km northwest of the volume observed by beam 2. During most of the measurement period, the wind direction was east-southeast in the 90-95 km altitude range, where the main portion of the Na layer was found. This means that when taking the time lag into account, the volumes seen by the two beams were relatively close. I estimate the average windspeed to be around 60 m/s, which would

indicate an expected time lag of 15 minutes at 54 km, which is close to what is observed.

Note that the minimum Na density in the colour plot is $750 \cdot 10^6/m^3$, which means lower densities are not plotted. I have studied all the plots at a minimum setting of 0 in order to see the full extent of the Na layer. My findings are given towards the end of this section.

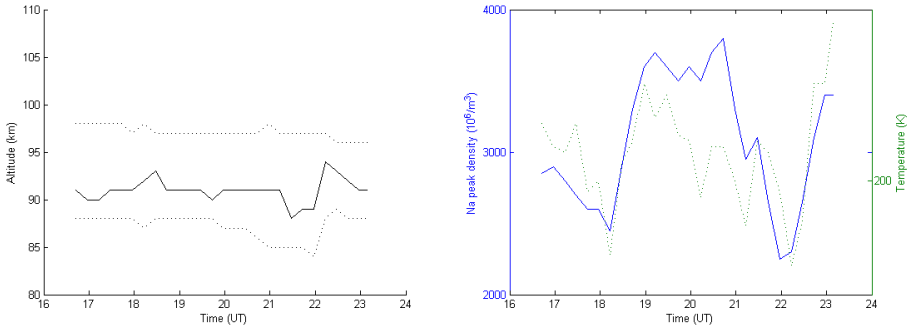

Figure 6: To the left, altitude of the Na density peak and the altitudes where the Na density is half the peak maximum. To the right, Na density and temperature at the Na density peak.

Figure 6 shows the altitude of the Na density peak during the measurement, and the values of the Na density and temperature at the peak. We see a global minimum in both Na density and temperature at around 22:15. The Na depletion is also clearly visible in the colour plot in figure 5. This is due to a gravity wave, the effects of which are clearly visible in the temperature plots as a sinking layer of colder atmosphere. There is another strong minimum in Na density and temperature at 18:15, which gives the gravity waves a period of 4 hours. The relatively warm time period between the minima coincides very well with the period of highest Na density. For the first four hours of the measurement, there is a temperature minimum at 87-88 km, which seems to be independent of the gravity wave. This can be interpreted as the mesopause. A temperature peak is seen in the 90-95 km interval at around 23:00, which is accompanied by the Na density recovering after the strong depletion. This is stronger in beam 2 than beam 1, but since the measurement ends shortly afterwards, we do not get to see how the Na density developed after this.

A wave structure is also visible in the windspeed data, particularly in beam 2. There are two ways to interpret the plot: A windspeed maximum that sinks from 105 km at 18:00 to 85 km at 22:00, which is close to the observed temperature minimum, or one that sinks from 95 km at 17:00 to 85 km at 22:00. There is typically a phase shift between the wind component and the temperature component of a gravity wave, so it would not be unexpected if the interpretation that deviates from the observed temperature minimum were accurate.

4 December

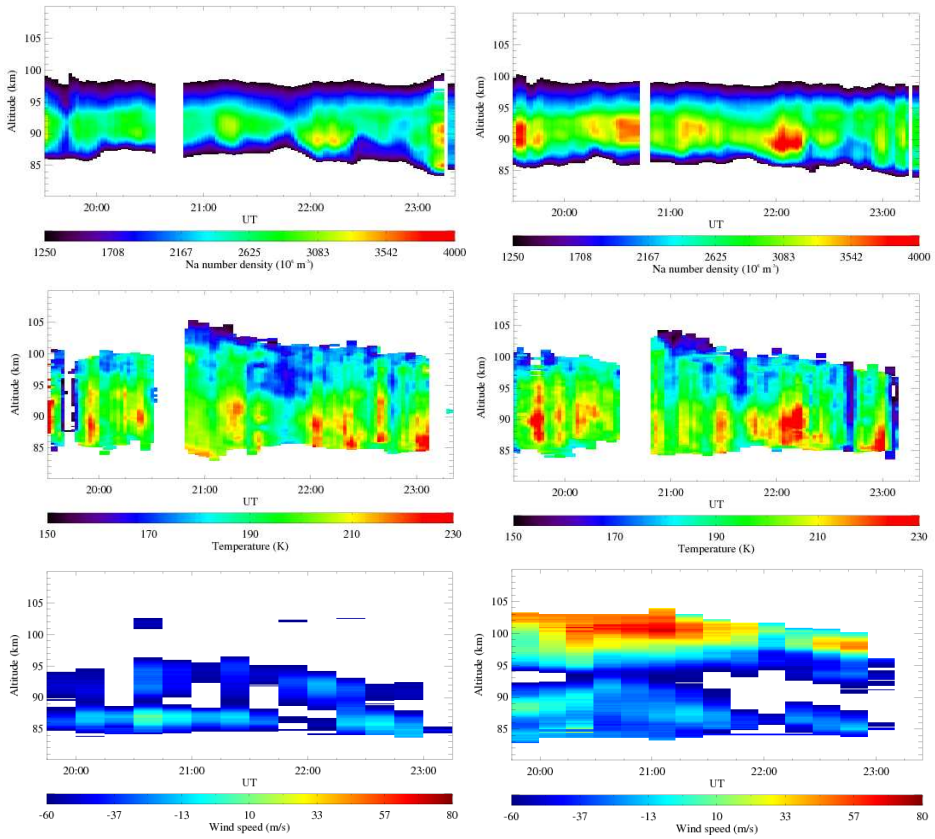

Figure 7: Na density (top), prelim. temperature (middle) and windspeed data (bottom) for 4 December 2010. Left row is from beam 1 (north), right row is from beam 2 (east).

ECOMA 7 launched at 04:21 on 4 December, about 16 hours before these measurements. We were unable to make lidar measurements during the launch because of a thick layer of clouds. In this dataset, we see periodic changes in both Na density and temperature, but there are no clearly visible gravity waves as in the data from 26 November, because these data cover a shorter altitude interval due to higher uncertainty. The interuption between 20:30 and 20:50 was because of a laser dye change in the pulsed dye amplifier (see section 1.4). The laser dye is generally replaced every 12-14 hours of system operation, and its age can significantly affect the quality of the received data, as is indicated by the increased altitude coverage in the temperature data after the interruption. The data from the two beams show the same tendencies, but are not as similar as the 26 November data. The wind data is of low quality, but indicates a wind direction in the southwest direction in the 85-95 km range, which is perpendicular to a line between the observed atmospheric volumes.

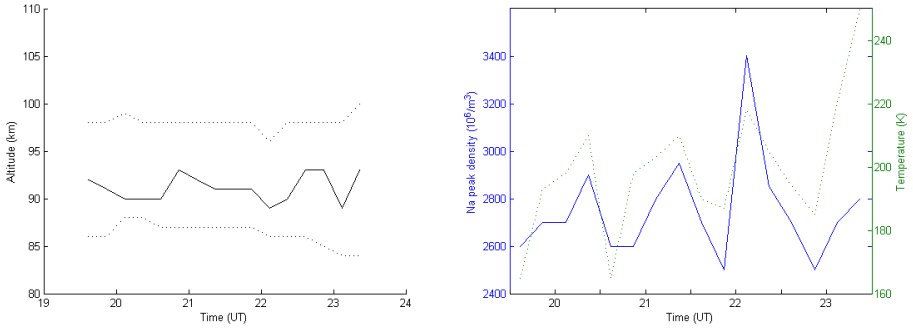

Figure 8: To the left, altitude of the Na density peak and the altitudes where the Na density is half the peak maximum. To the right, Na density and temperature at the Na density peak.

5 December, morning

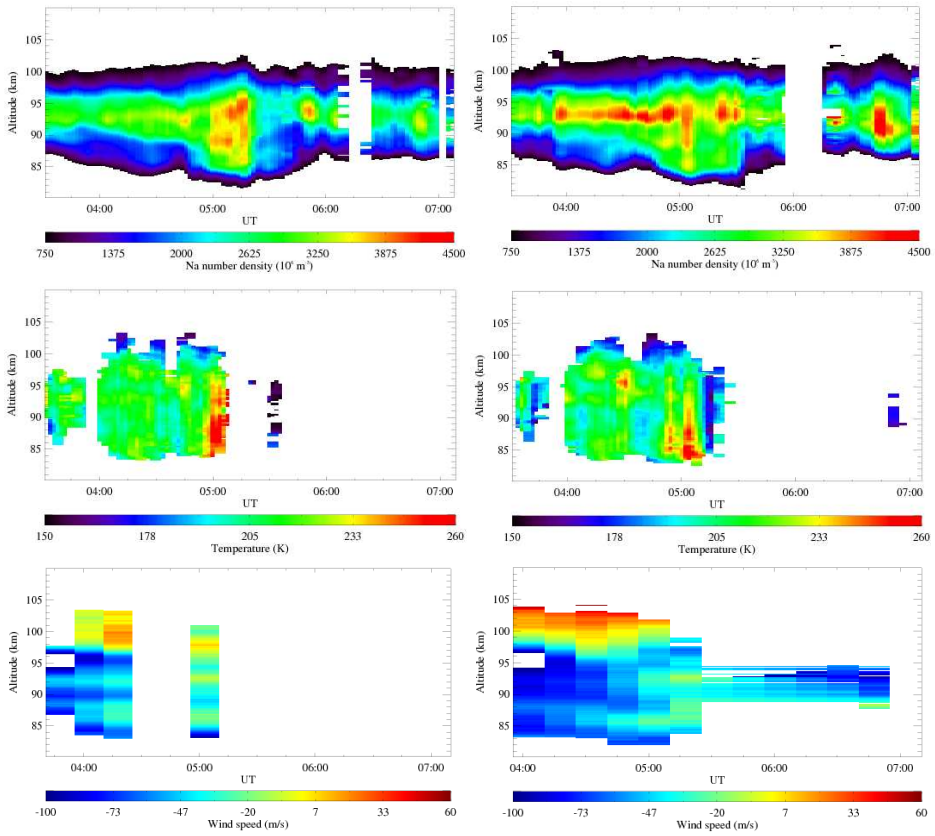

Figure 9: Na density (top), prelim. temperature (middle) and windspeed data (bottom) for 5 December 2010. Left row is from beam 1 (north), right row is from beam 2 (east).

The data from the morning hours of 5 December are of low quality, likely because of a thin cloud layer, and only provide temperature data for the first half of the measurement. This is too poor to make a useful plot of the Na density and temperature at the Na density peak. From 03:30 to 05:00, both the temperature and the Na density appear stable. Shortly before 05:00 we see in beam 1 a strong temperature increase in the 85-95 km range, accompanied by a strong Na density enhancement. At the most, we see an Na density above $2000m^{-3}$ from 84 to 98 km, with a peak of 4700 at 95 km. At 05:20, this enhancement is quickly depleted, but we do not have any reliable temperature data beyond this point. In beam 2, we also see a temperature increase shortly before 04:00, but it is not as strong above 90 km, and the

accompanying Na density enhancement primarily consists of a widening of the main portion of the layer (as in beam 1, densities above $2000m^{-3}$ between 84 and 96 km) while the density maximum remains largely unchanged. We see a sudden depletion at 05:35, which is about 15 minutes later than in beam 1. In both beams, we see some local Na density maxima of significant magnitude, but we do not have any temperature data to compare with. The wind data indicate a threshold at about 98 km, with a weak northeastern wind above it, and a a strong southwestern wind below it.

5 December, evening

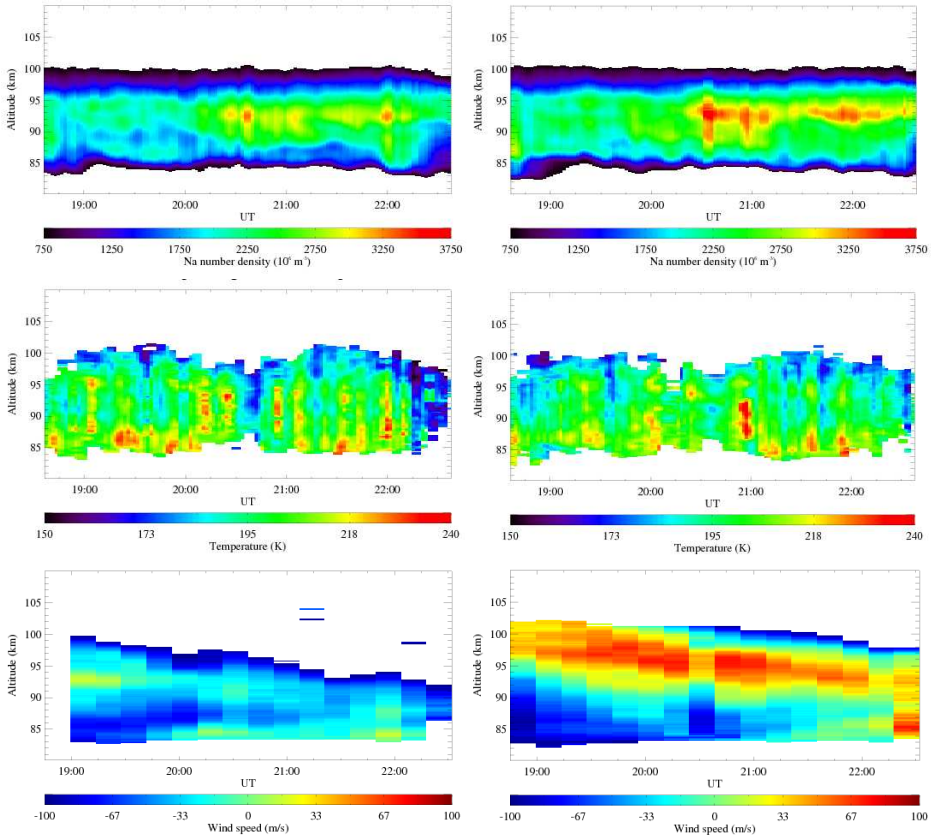

Figure 10: Na density (top), prelim. temperature (middle) and windspeed data (bottom) for 5 December 2010. Left row is from beam 1 (north), right row is from beam 2 (east).

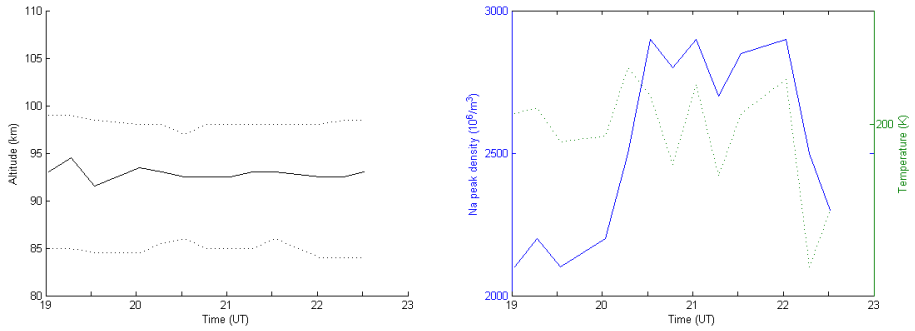

Figure 11: To the left, altitude of the Na density peak and the altitudes where the Na density is half the peak maximum. To the right, Na density and temperature at the Na density peak.

Measurement conditions improved during the day of 5 December, giving us higher quality data throughout the evening. We see several local Na density maxima, most of which accompany a local temperature maximum. There are no clear wave structures in the temperature data, but we see too little above 95 km to dismiss their existence. Wind data from beam 2 show a slowly sinking layer of strong eastwards wind, which indicates the presence of long-period gravity waves. At 22:15 there is a sudden temperature decrease over the entire altitude interval, and the main portion of the Na layer narrows to 91-96 km. There is no Na layer broadening in beam 2, but we see a similar temperature drop and Na layer narrowing at 22:30. The measurement ends before we get to see how this develops.

7 December

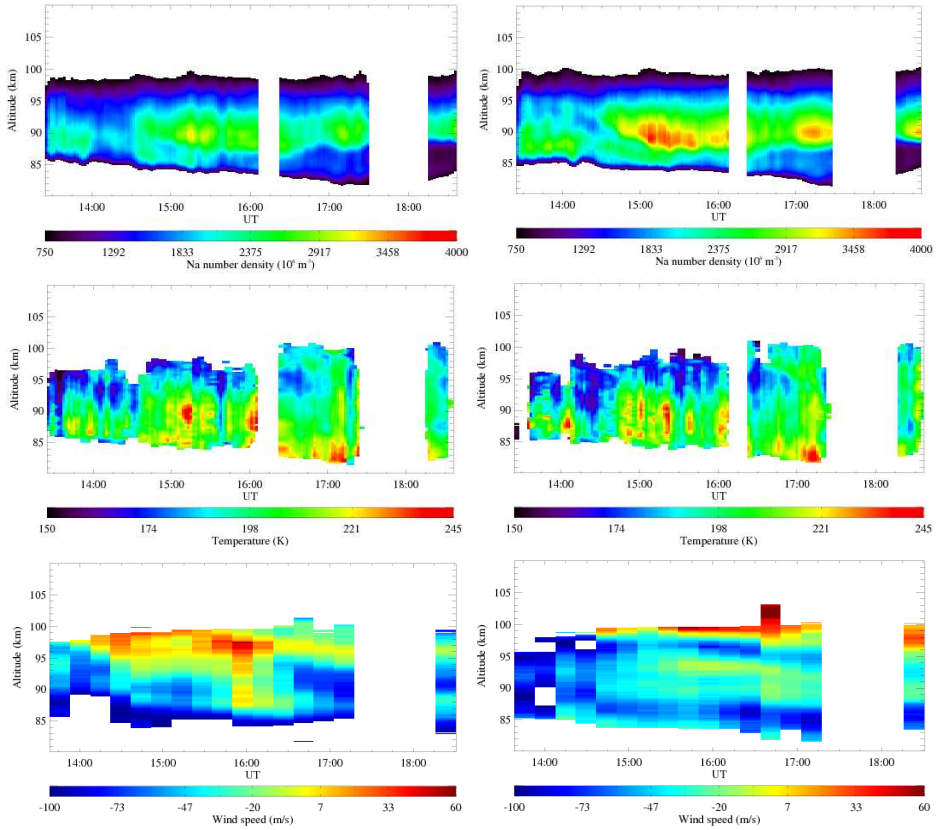

Figure 12: Na density (top), prelim. temperature (middle) and windspeed data (bottom) for 7 December 2010. Left row is from beam 1 (north), right row is from beam 2 (east).

For the first hour of this measurement, the main portion of the Na layer is weak and narrow, while the temperature in the 90-95 km range is roughly 30 K lower than below 90 km. At about 14:40, we see a rapid temperature increase of around 20 K in beam 1 and 25 K in beam 2. The temperature data cover too short an altitude interval to properly indicate whether this is is due to a gravity wave, but this could be due to a temperature minimum moving upwards. This temperature increase is accompanied by a significant Na density enhancement, .

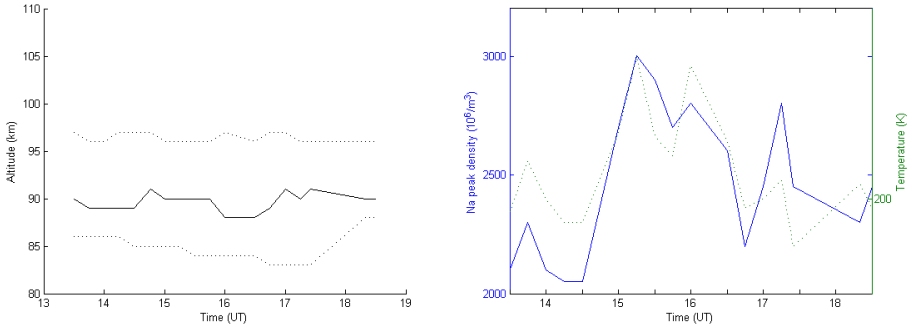

Figure 13: To the left, altitude of the Na density peak and the altitudes where the Na density is half the peak maximum. To the right, Na density and temperature at the Na density peak.

13 December

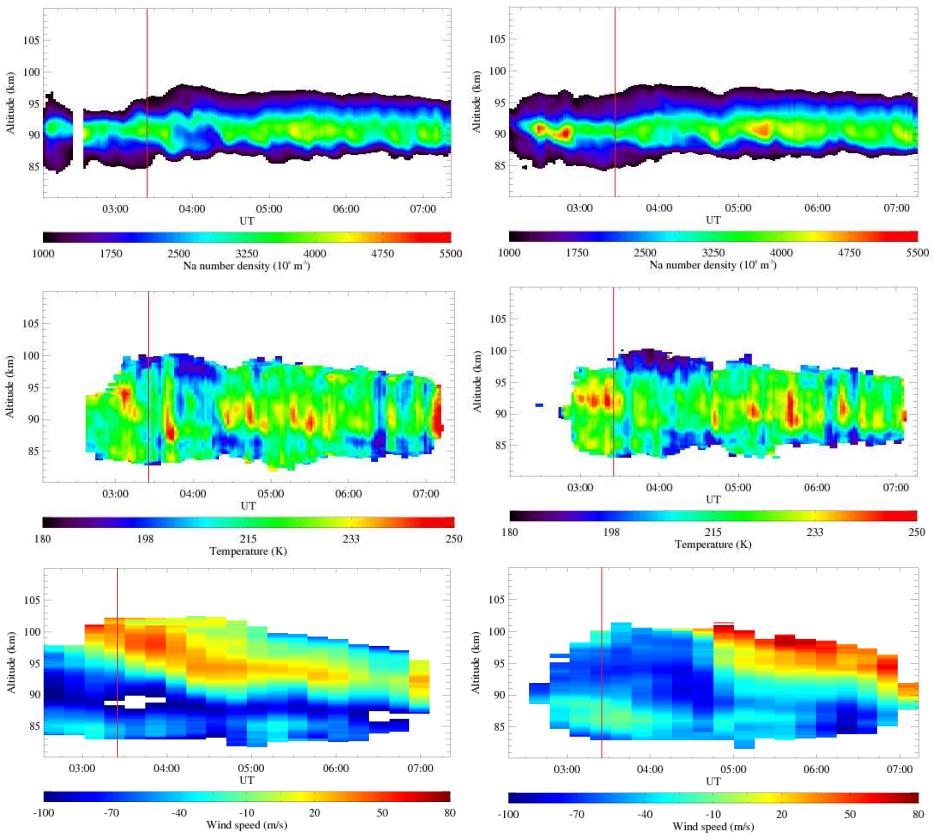

Figure 14: Na density (top), prelim. temperature (middle) and windspeed data (bottom) for 13 December 2010. Left row is from beam 1 (north), right row is from beam 2 (east).

Compared to the other measurements from the ECOMA 2010 campaign, the 13 December data show an overall dense and narrow Na layer, with large density and temperature variations. Figure 15 shows a mean full width at half maximum (FWHM) of about 7 km. There is a strong Na depletion at 03:50, which is stronger in the lower part of the layer. This causes the density peak to move upwards.

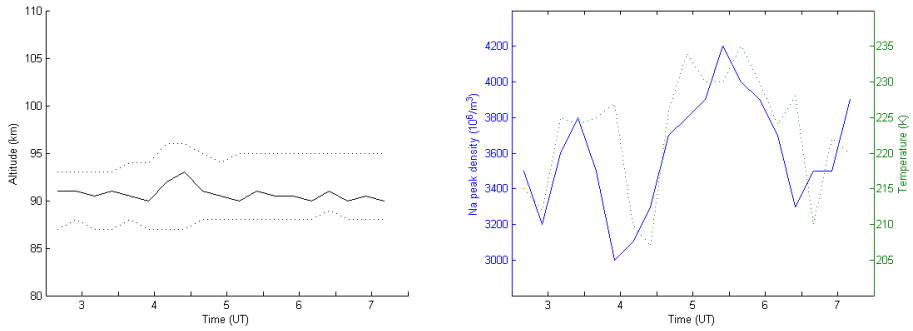

Figure 15: To the left, altitude of the Na density peak and the altitudes where the Na density is half the peak maximum. To the right, Na density and temperature at the Na density peak.

ECOMA 8 was launched 3:24 this day, and the individual height profiles for Na density, temperature and windspeed are given in figures - . At the time of launch, the atmosphere is fairly stable in the Na layer altitude range. There is an interesting element in the temperature data, with a roughly constant 25 K difference in the two beams, which is quite large. However, as mentioned earlier, the horizontal distance between the two atmospheric volumes seen by the two beams, is 49 km at 95 km altitude, which translates to a $0.5°/km$ horizontal temperature gradient, which is not unlikely.

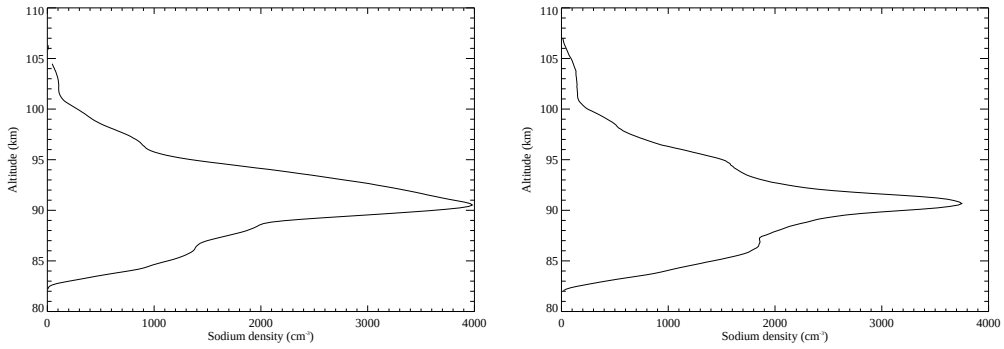

Figure 16: Na density profiles for the ECOMA 8 launch, 03:24 December 13th, 2010. North beam is shown to the left, and east beam to the right. 5 minutes integration period.

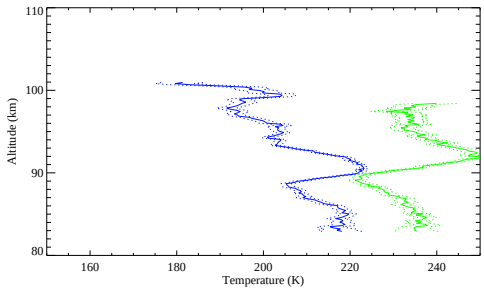

Figure 17: Prelim. temperature profiles for the ECOMA 8 launch. North beam is shown as blue, and east beam as green. 5 minutes integration period.

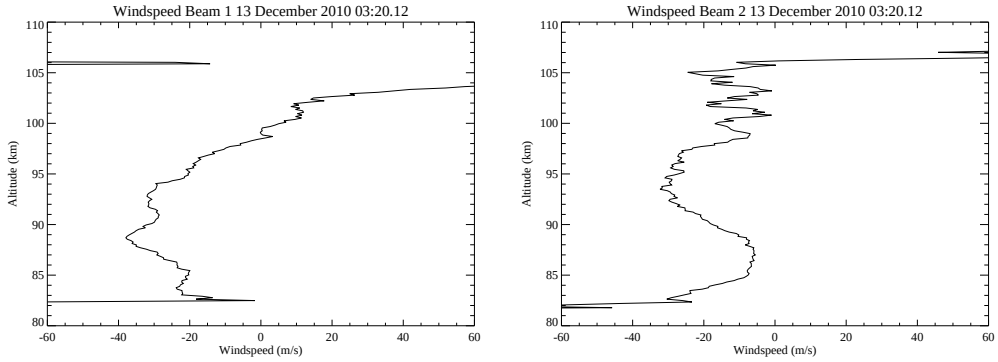

Figure 18: Windspeed profiles for the ECOMA 8 launch. North beam is shown to the left, and east beam to the right. 15 minutes integration period.

19 December, morning

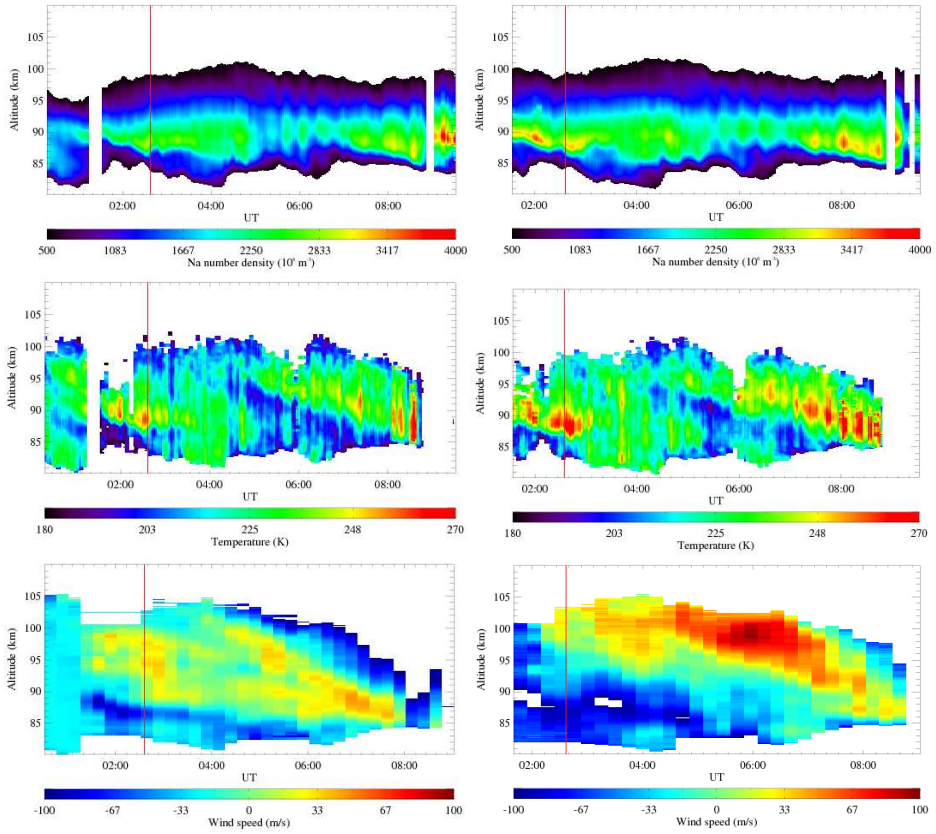

Figure 19: Na density (top), prelim. temperature (middle) and windspeed data (bottom) for 19 December 2010. Left row is from beam 1 (north), right row is from beam 2 (east).

On 19 December, we made measurements for a total of 18.5 hours under good conditions. The dataset is split in two parts, morning and afternoon, to make it easier to display the results. This is the second dataset (26 November being the first) to clearly show the presence of a wave structure, with two temperature maxima at around 02:00 and 08:00 in 87-92 km altitude (giving a period of 6 hours). ECOMA 9 was launched at 2:36 in the morning, as shown by the red line in the plots of figure 19.

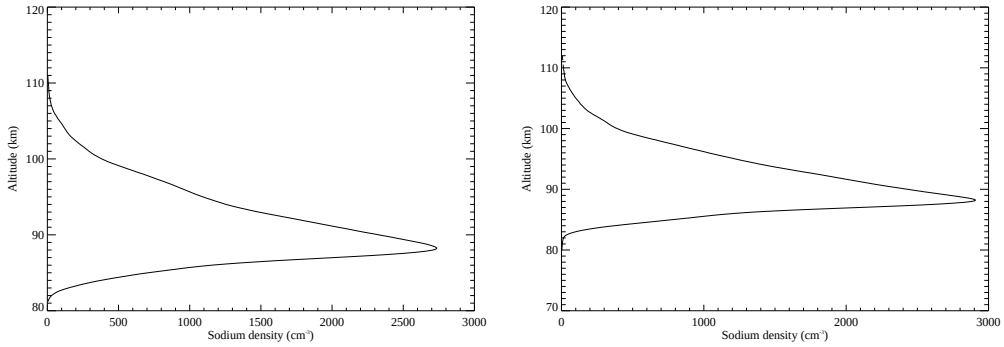

Figure 20: Na density profiles for ECOMA 9 launch, 02:36 December 19th, 2010. Left: North beam, right: East beam. 5 minutes integration period.

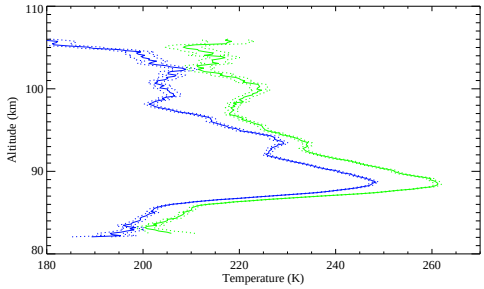

Figure 21: Prelim. temperature profiles for the ECOMA 9 launch. North beam is shown as blue, east beam as green. 5 minutes integration period.

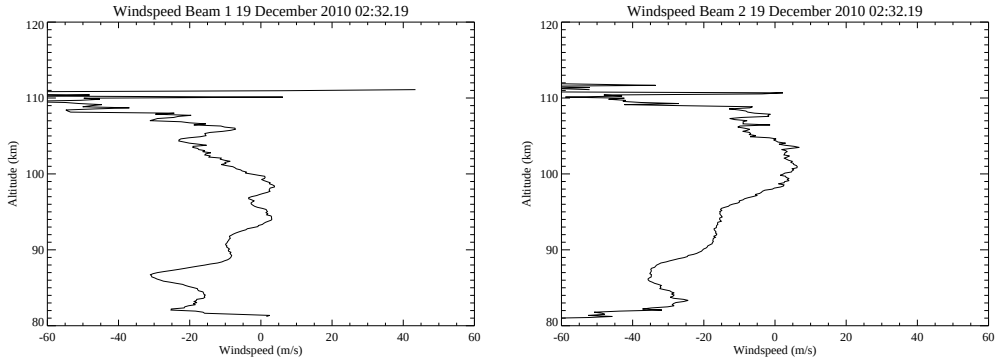

Figure 22: Windspeed profiles for the ECOMA 9 launch. North beam is shown to the left, and east beam to the right. 15 minutes integration period.

19 December, afternoon

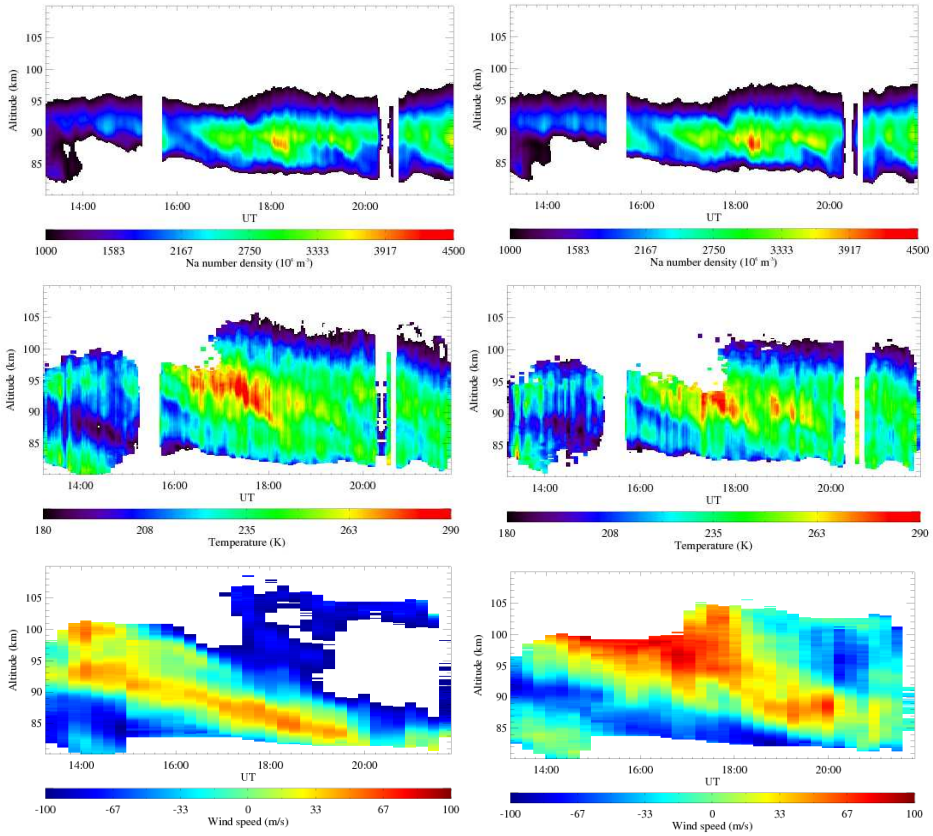

Figure 23: Na density (top), prelim. temperature (middle) and windspeed data (bottom) for 19 December 2010. Left row is from beam 1 (north), right row is from beam 2 (east).

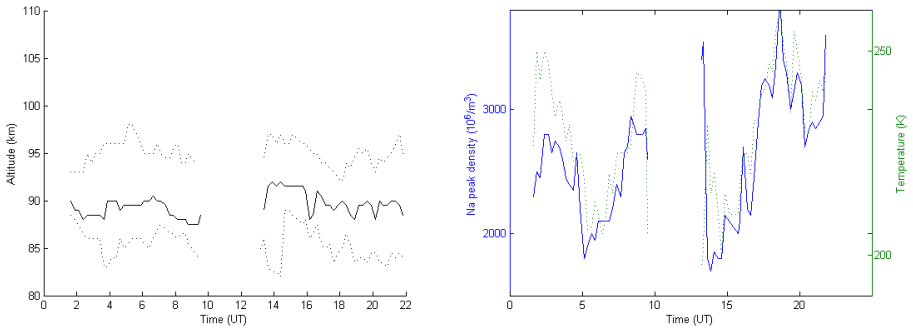

Figure 24: To the left, altitude of the Na density peak and the altitudes where the Na density is half the peak maximum. To the right, Na density and temperature at the Na density peak. Includes both the morning and afternoon dataset from 19 December.

Day	Measurement period (UT)	Layer boundaries (km) Min.	Max.
26 November	16:36-23:13	85-100	80-105
4 December	19:30-23:34	86-103	83-105
5 December	03:25-07:40	85-105	84-105
5 December	18:36-22:37	82-103	82-104
7 December	13:24-18:37	85-102	81-104
13 December	02:03-07:23	85-97	83-100
19 December	00:17-10:09	84-100	81-102
19 December	13:12-21:52	85-99	81-102

Table 2: Na layer boundary heights during minimal and maximal layer thickness for each dataset. Total measurement time of 48 hours.

Summary of measurements during ECOMA 7-9

Table 2 shows that if the measurements from the ECOMA/Geminids campaign period provided representative data, the Na layer between November 25th and December 20th will typically have a lower boundry at 81-85 km, and an upper boundary at 100-104 km. I find a mean peak altitude of 91.3 km, a mean Na peak density of $2800 \cdot 10^6/m^3$, and a mean FWHM of 9.4 km. These numbers are calculated by using the same data points as I used in the peak altitude and density-temperature plots for each dataset. The Na density peak is normally below the center of the FWHM interval, at a mean of 3.7 km above the lower FWHM boundary altitude.

3 Sudden Na layers

3.1 Characteristics of sudden sodium layers

Na is deposited in the atmosphere by meteors ablating during entry, at a global rate of 10-100 tons per day (Love and Brownlee, 1993; Gabrielli et al., 2004). Since it is an alkali metal and highly reactive, sodium is normally chemically bound to other elements such as $NaHCO_3$ in the lower, denser parts of the atmosphere, while in the higher parts it tends to be ionized due to charge transfer from NO^+ and O_2^+ and a small degree of solar photoionization (Plane, 2003). At approximately the 80-110 km altitude range, Na can be found in atomic, non-ionized form, which is referred to as the Na layer. The number density of Na atoms has a seasonal variation, with a maximum in winter; at polar latitudes the winter density is a factor 10 larger than the summer density, while this factor gets smaller at lower latitudes and is around 1.3 close to the equator. The seasonal variation is assumed to be due to Na depletion caused by the lower mesospheric temperatures in summer and to photochemical effects in polar summer. The peak density is usually around 88 km in winter and 92 km in summer.

In addition to the seasonal variation of the Na density, we observe variations of the same order of magnitude, but in much smaller time scales. These density increases are called sporadic or sudden sodium layers (SSLs), and typically have 2-20 times as high density as the background density while covering an altitude interval of about 2 km (Clemesha, 1995). They can appear in a matter of minutes and last for several hours before disappearing just as quickly (Gardner et al., 1995; Kaifler (2009)) or slowly fading away (Heinrich et al., 2008). SSLs may extend horizontally from about 100 km to several thousand km; it should be noted that from the perspective of a stationary lidar it is impossible to tell whether the appearance of an SSL is due to wind transport or actual formation of the sudden layer, but it is assumed that wind transport dominates (Batista et al, 1991). At high latitudes, they occur far more often during summer than winter, with a factor of around 10 in the polar regions. There is also a strong dependency of local time, with the majority of observations made at ALOMAR between 2000-2006 being within two hours of local midnight (Heinrich et al., 2008).

3.2 Temperature dependent formation processes

Simultanous observations of Na density and temperature of the Na layer suggest that temperature has an effect on the balance between formation and loss of atomic Na. Plane and Rajasekhar (1989) state that the reaction between Na atoms and oxygen molecules

$$Na + O_2 + N_2 \longrightarrow NaO_2 + N_2 \tag{1}$$

is a very important sink of atomic Na in the mesosphere. Being a part of NaO_2, the Na atom can no longer absorb and re-emit photons of the same wavelengths as the photons from the Na lidar, and it becomes invisible to our receiver. Laboratory experiments show that the rate coefficient of reaction (1) is proportional to $T^{-1.3}$. An increase in temperature causes reaction (1) to slow down, and the Na density increases because of a weaker loss process. Zhou et al. (1993) found that a temperature increase of 10 K can lead to a doubling of Na density, and further suggest that if the windshear mechanism, as decribed in section 3.3 is present within the Na layer due to tidal winds, while acousto-gravity waves propagate through it, the combination of increased ion density (specifically Na^+) and a positive temperature fluctuation creates a sudden Na layer. Data from the Na lidar show that temperature fluctuations of up to $\pm 20K$ are not uncommon (see section 2.3 for examples).

3.3 Other formation processes

Nesse et al (2008) describe four of the most probable theories behind the formation of SSLs, one of which consider the temperature dependent mechanisms I have discussed in section 3.2. I briefly describe the other three theories in the following subsections.

Deionization of Na ions in sporadic E-layers

Sporadic E-layers are generally thin layers of metallic ions, such as Fe^+, Na^+ and Mg^+, that typically occur between 90 and 140 km altitude. One

theory is that Na ions from the E-layer convert into atomic Na as the E-layer sinks to lower altitudes, through a complex set of chemical reactions with other substances. These substances can be N_2, O_2 or CO_2 (Cox and Plane, 1998). Heinrich et al. (2008) have studied the SSL events observed with the ALOMAR Na lidar with specific focus on the connection with E-layers using ionograms from the EISCAT Tromsø Dynasonde. In all 9 cases E-layers were observed within 20 minutes of the onset of a SSL observed at ALOMAR. Hansen and von Zahn (1990) describe a convincing correlation between the formation of E-layers and SSLs, where the E-layers have a very strong tendency to form before the SSLs and at higher altitudes. Mathews (1998) describes some likely formation processes for E-layers, such as the windshear mechanism described below, though full understanding has not yet been accomplished. Nygren et al. (1984) suggest that strong auroral electric fields can play roughly the same role as windshear and rapidly create an E-layer, which can contain Na^+ forming a basis for a neutral Na layer.

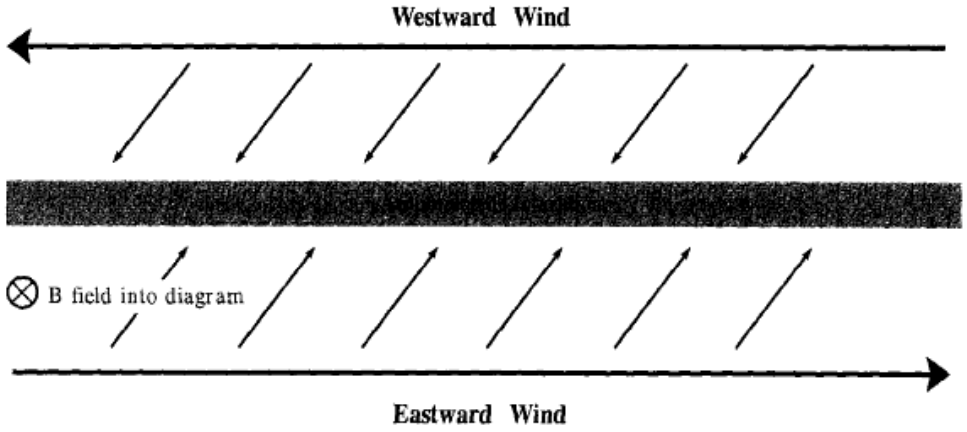

1.) $0 = e(\mathbf{v}_i \times \boldsymbol{B} + \boldsymbol{E}) - M\nu_{in}(\mathbf{v}_i - \boldsymbol{V}_n)$ — Steady-state ion momentum equation.

2.) $\mathbf{v}_i = (u, v, w)$; $\boldsymbol{V}_n = (U, V, 0)$ — Ion and neutral velocity vectors in magnetic south, east, and upward directions.

3.) $\boldsymbol{B} = -B_0(\cos I, 0, \sin I)$ — Magnetic field vector (dip angle I; magnitude B_0).

4.) $w = \dfrac{U\cos I \sin I + rV\cos I}{1 + r^2}$ — Ion vertical speed for electric field $\boldsymbol{E}$=0.

5.) $r = \nu_{in}/\omega_{ci}$ — Ratio of ion-neutral collision frequency (ν_{in}) to ion-cyclotron frequency ($\omega_{ci} = eB_0/M$) for an ion of mass M and electron-charge e.

Fig. 1. A graphical summary of and basic equations for the "windshear" ion layer formation mechanism.

Figure 25: A graphical summary of and basic equations for the "windshear" ion layer formation process. (Mathews, 1998, figure 1)

Mathews (1998) describe how the wind shear mechanism can cause dense ion layers in the mesosphere. The windshear theory can be described in short like this: Picture two adjacent atmospheric layers in the ionosphere, where the upper layer has a westward wind, while the lower layer has an eastward wind. This is illustrated in figure 25. These motions combined with the Earth's northward magnetic field create a **V**x**B** drift of the positive ions (**V** is the wind vector, while **B** is the magnetic field vector), which is directed downwards in the upper layer, and upwards in the lower layer. The result is an increased ion density along the border of the two layers, which is referred to as a sporadic E-layer if it is in the E region. This principle also applies to two atmospheric layers where the wind is westwards in both, but the wind is weaker in the lower layer; the lower layer receives ions from the upper layer faster than it deposit ions downwards, and the ion density gradually increases. In two layers with eastwards winds, this process takes place if the wind is weaker in the upper layer; the upper layer receives ions from the lower level faster than it can deposit ions upwards. Windshear is sufficient to describe E-layers occuring at mid-latitudes, but at high-latitudes such as at Andøya, the magnetic field is significantly inclined downwards, and the nortwards component is smaller, which slows down this process. Kirkwood and von Zahn (1993a, b) show that an electrical field with a southward component is required as well as the described wind structure.

Increased meteoric deposition

Since meteors are the source of Na in the upper atmosphere, it is a natural assumption that a larger mass of incoming meteors would likely cause an increased Na density. Clemesha et al. (1978) suggested that SSLs could be caused by single large meteors ablating during entry, while Clemesha et al. (1988) described how an initially thick Na layer, caused by meteor deposition, could be changed into a narrower and denser layer through the windshear mechanism. Meteors ablating in the atmosphere leave a trail of ionized particles called meteor echoes, which can be observed using radar. Nesse et al. (2008) studied one particular SSL occuring on 5 November 2005 and compared the number of meteor echoes observed by the All-Sky Interferometric Meteor Radar (SKiYMET), which is located at the Andøya Rocket Range, with the number of meteor echoes prior to the SSL. They found that the number of meteors was slightly less than the monthly average prior to the event, and while they could not rule out the possibility that a single large meteor had caused the increased abundance of Na, there was no

increased probablility that this was the case. Hansen and von Zahn (1990), and Batista et al. (1989) have investigated the possibility of a correlation between meteor showers and SSLs, but found no conclusive evidence.

Auroral electron precipitation of meteoric smoke particles

When entering the atmosphere, meteors ablate and form meteoric smoke particles through re-condensation and coagulation. In addition to consisting of about 1% Na (Donahue and Meier, 1967), these can adsorb Na ions, atoms and molecules consisting of Na, during their slow sedimentation through the Na layer. von Zahn et al. (1987) proposed that electrons during auroral events can act on the surface of the smoke particles and cause them to release atomic Na. If some appropriate meteorological processes are present, such as the windshear mechanism described above, the smoke particles would form a narrow layer which would translate into a narrow Na layer as the Na atoms were released from the smoke particles.

This theory explains the correlation between SSLs and low-altitude E-layers, since the meteoric smoke particles would also function as a source of metallic ions in addition to neutral Na. However, the theory cannot explain SSLs at latitudes without significant auroral activity, and observations of SSLs and E-layers have been made in periods without auroral activity at high latitudes. This does not mean that individual SSL events cannot be primarily driven by this process, but that it cannot be main factor of the SSL phenomena in general. A similar theory is presented by Beatty et al. (1989), who suggest that it is collisions with the ions of the E-layer which cause the smoke particles to release Na atoms, instead of auroral electrons.

3.4 Example of sporadic Na layer

Kaifler (2009) recorded a sporadic Na layer close to midnight between January 26 and January 27 2009, above the regular Na layer. This is close to the same time of year as the measurements made during ECOMA/Geminids, and the data is of high quality and allow good temperature data at the relevant altitudes. I investigate whether a temperature dependent formation process such as the one described in section 3.2 could be a likely source for this layer. Na density and temperature from the measurement are shown in

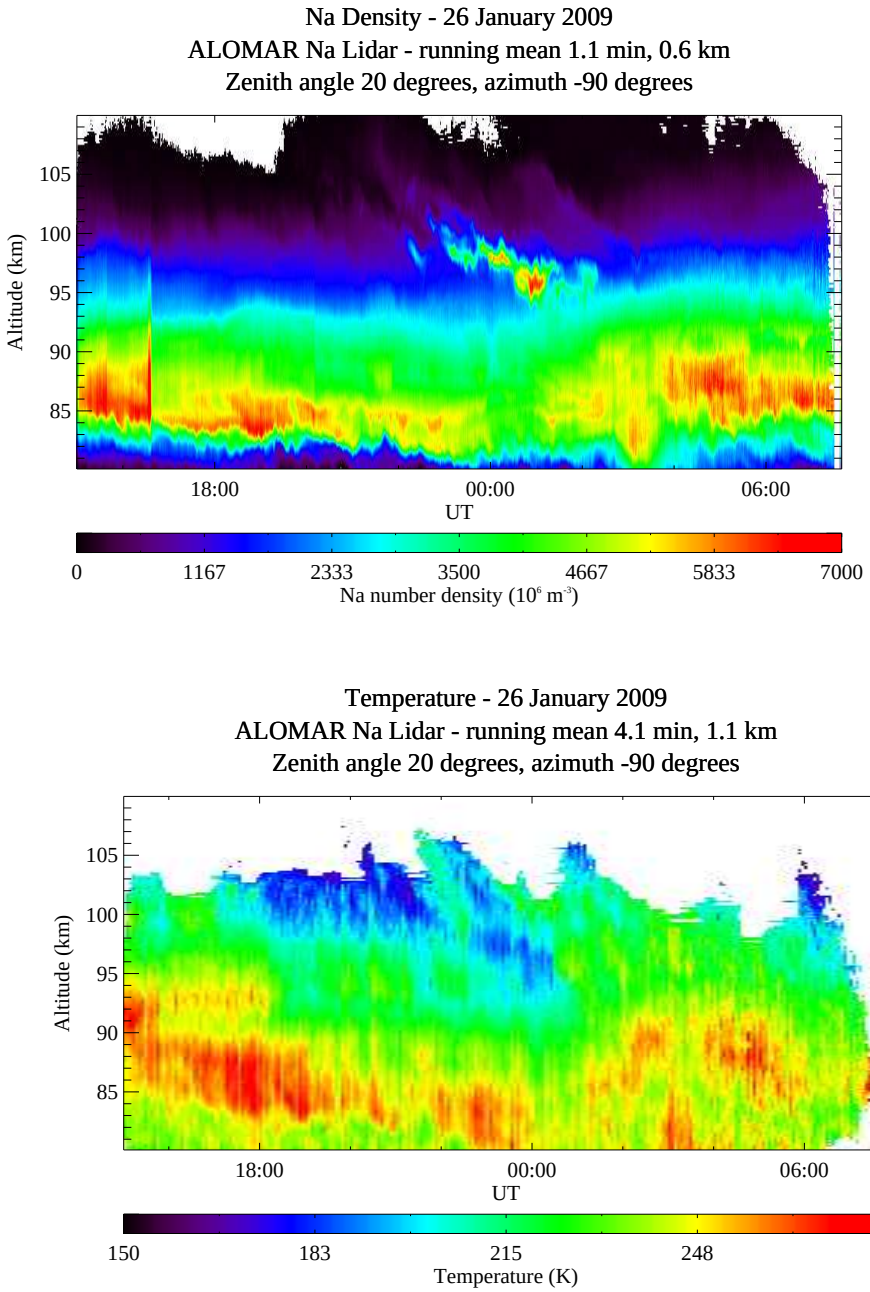

Figure 26: Top: Na density plot of a sporadic Na layer measured at 26 and 27 January 2009. Bottom: Prelim. temperature plot of the same sporadic Na layer.

figure 26. The lidar measured with one beam towards west and one towards east; I present only the data from the east beam here because the SSL was stronger.

The plots indicate that a temperature dependent mechanism behind the formation of this particular layer is unlikely as there are no nearby hotspots. In fact, the onset of the SSL is within an area which is significantly colder than the surroundings. I use a four minutes integration time to create a plot with the Na density and temperature at the Na peak, as I did with the datasets in section 2.3. I also record the Na peak altitude, but I do not measure the FWHM because the SSL signal overlaps the signal from the regular Na layer.

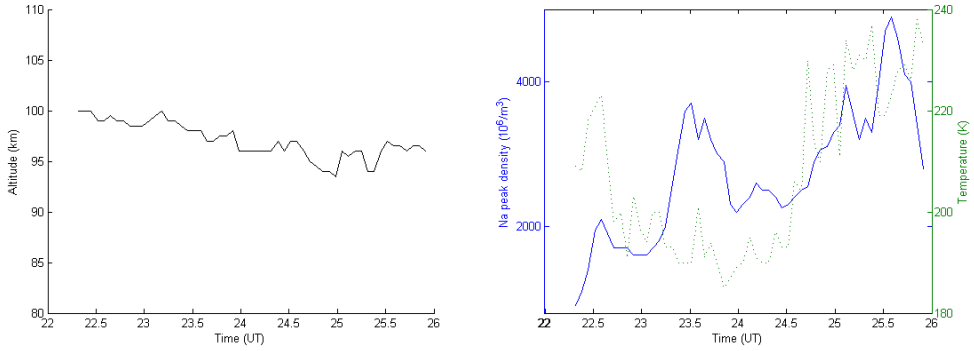

Figure 27: To the left, altitude of the Na density peak of a sporadic Na layer measured at 26 and 27 January 2009. To the right, Na density and temperature at the Na density peak.

The results are displayed in figure 27. While the Na density maximum between 00:30 and 02:00 coincides with an increase in temperature, the rest of the Na density development does not appear to be connected to the temperature. It's likely that if the conditions were favourable to a temperature dependent formation process, it would have contributed to the Na abundance, but it did not dominate the process. A more likely theory which fits this case better, is deionization of Na^+ from a sporadic E-layer as described in section 3.3 because the SSL is sinking from a higher altitude. Above about 100 km, ionized Na has a lifetime of more than a day, but this decreases to just a few minutes at 90 km (Collins et al., 2002), and this layer sinks from about 100 km to 95 km. It also seems to fit with the increased Na peak level at the lower altitudes.

References

- Batista, P. P., Clemesha, B. R., Batista, I. S., and Simonich, D. M.: Characteristics of the sporadic sodium layers at 23° S, J. Geophys. Res., 94, 15 349-15 358, 1989.

- Batista, P. P., Clemesha, B. R., and Simonich, D. M.: Horizontal structures in sporadic sodium layers at 23° S, Geophys. Res. Lett, 18, 1027-1030, 1991.

- Beatty, T. J., Collins, R. L., Gardner, C. S., Hostetler, C. A., Sechrist, C. F., and Tepley, C. A.: Simultaneous radar and lidar observations of sporadic E and Na layers at Arecibo, Geophys. Res. Lett. 16, 1019-1022, 1989.

- Clemesha, B. R., Kirchhoff, V.W. J. H., Simonich, D. M., and Takahashi, H.: Evidence of an extraterrestrial source for the mesospheric sodium layer, Geophys. Res. Lett., 5, 873-876, 1978.

- Clemesha, B. R., Batista, P. P., and Simonich, D. M.: Concerning the origin of enhanced sodium layers, Geophys. Res. Lett., 16, 1267-1270, 1988.

- Clemesha, B. R.: Sporadic neutral metal layers in the mesosphere and lower thermosphere, J. Atmos. Terr. Phys, 57, 725-736, 1995.

- Collins, S. C., Plane, J. M. C., Kelley, M. C., Wright, T. G., Soldn, P., Kane, T. J., Gerrard, A. J., Grime, B. W., Rollason, R. J., Friedman, J. S., Gonzlez, S. A., Zhou, Q., Sulzer, M. P. and Tepley, C. A.: A study of the role of ion-molecule chemistry in the formation of sporadic sodium layers, Journal of Atmospheric and Solar-Terrestrial Physics, 64(7), 845 - 860, doi:DOI:10.1016/S1364-6826(02)00129-3, 2002.

- Cox, R. M. and Plane, J. M. C.: An ion-molecule mechanism for the formation of neutral sporadic Na layers, J. Geophys. Res., 103, 6349-6359, 1998.

- Donahue, T. M. and Meier, R. R.: Distribution of sodium in the daytime upper atmosphere as measured by a rocket experiment, J. Geophys. Res., 72, 2803, 1967.

- Fricke, K. H. and von Zahn, U.: Mesopause temperatures derived from probing the hyperline structure of the D2 resonance line of sodium by

lidar, Journal of Atmospheric and Terrestrial Physics, Vol 41, No 5, 499-512, 1985.

- Fritts, D. C., and Alexander M. J.: Gravity wave dynamics and effects in the middle atmosphere, Rev. Geophys., 41(1), 1003, doi:10.1029/2001RG000106, 2003.

- Gabrielli, P., Plane, J. M. C., Varga, A., Hong, S., Cozzi, G., Gaspari, V., Planchon, F. A. M., Cairns, W., Ferrari, C., Crutzen, P., Cescon, P., and Boutron, C. F.: Meteoric smoke fallout over the Holocene epoch revealed by iridium and platinum in Greenland ice, Nature, 432, 1011-1014, 2004.

- Gardner, C. S., Tao, X., and Papen, G. C.: Observations of strong wind shears and temperature enhancements during several sporadic Na layer events above Haleakala, Geophys. Res. Lett., 22, 2809-2812, 1995.

- Gibson, A. J., Thomas, L., Bhattachacharyya, S. K.: Laser observations of the ground-state hyperfine structure of sodium and of temperatures in the upper atmosphere, Nature, 281, 131-132, 1979.

- Hansen, G., von Zahn, U.: Sudden sodium layers in polar latitudes, Journal of Atmospheric and Terrestrial Physics, Vol. 52, No. 6-8, 585-608, 1990.

- Heinrich, D., Nesse, H., Blum, U., Acott, P., Williams, B., and Hoppe, U.-P.: Summer sudden Na number density enhancements measured with the ALOMAR Weber Na Lidar, Ann. Geophys., 26, 1057-1069, 2008.

- Heinrich, D.: Temperature and sodium density studies in the Arctic mesopause region based on measurements with the ALOMAR Weber Sodium Lidar, PhD thesis submitted to the Department of Physics, University of Oslo, 2007.

- Holton, J. R.: An Introduction to Dynamic Meteorology, ISBN 9780123540157, Elsevier Science & Technology, 2004.

- Hoppe, U.-P.: The effects of gravity waves on horizontal layers: Simulation and interpretation, Proc, Ninth ESA/PAC Symposium on 'European Rocket and Balloon Programmes and Related Research', Lahnstein, FRG. 3-7 April 1989 (ESA SP-291. June 1989).

- Kaifler, B.: Na Lidar at ALOMAR - electrooptic improvements, analysis algorithms, and selected atmospheric observations 80 to 100 km above Northern Norway, thesis submitted for the Degree of Diplomphysiker in the University of Ulm, 2009. http://www.mil.no/ multimedia/archive/00132/ Bernd_Kaifler_2009__132532a.pdf

- Kirkwood, S. and von Zahn, U.: Formation mechanisms for low-altitude sporadic-E layers - results from the METAL campaign, 11th ESA Symposium on European Rocket and Balloon Programmes and Related Research, ESA SP-355, Montreux, Switzerland, 1993a.

- Kirkwood, S. and von Zahn, U.: Formation mechanisms for low-altitude E_S and their relationship with neutral Fe layers: Results from the METAL campaign, Journal of Geophysical Research 98, 21 549-21 561, 1993b.

- Love, S. G. and Brownlee, D. E.: A direct measurement of the terrestrial mass accretion rate of cosmic dust, Science, 262, 550-553, 1993.

- Mathews, J. D.: Sporadic E: Current views and recent progress, Journal of Atmospheric and Solar-Terrestrial Physics, Vol. 60. No. 4, pp. 413-435, 1998.

- Nesse, H., Heinrich, D., Williams, B., Hoppe, U.-P., Stadnes, J., Rietveld, M., , Singer, W., Blum, U., Sandanger, M. I., and Trondsen, E.: A case study of a sporadic sodium layer observed by the ALOMAR Weber Na lidar, Ann. Geophys., 26, 1071-1081, 2008.

- Nygren, T., Jalonen, L., and Huuskonen, A.: Density profiles of sporadic E-layers containing two metal ion species, J. atmos. terr. Phys. 46, p. 885-893, 1984.

- Prölss, G. W.: Physics of the Earth's Space Environment, An Introduction, ISBN 3-540-21426-7, Springer Berlin Heidelberg New York, 2004.

- Plane, J. M. C. and Rajasekhar, B.: Kinetic study of the reactions Na+O2+N2 and Na+N2 over an extended temperature range, J. Phys. Chem., 93, 3135-3140, 1989.

- Plane, J. M. C.: Atmospheric chemistry of meteoric metals. Chem. Rev., 103, 4963-4984, 2003.

- von Zahn, U., von der Gathen, P., and Hansen G.: Forced release of sodium from upper atmospheric dust particles, Geophys. Res. Lett., 14, 76-79, 1987.

- Sandford, M. C. W. and Gibson, A. J.: Laser radar measurements of the atmospheric sodium layer, Journal of Atmospheric and Terrestrial Physics, Vol 32, 1423-1430, 1970.

- She, C. Y., Yu, J. R., Latifi, H., and Bills, R. E.: High-spectral-resolution fluorescence light detection and ranging for mesospheric sodium temperature measurements, Applied Optics, Vol 31, No 12, 2095-2106, 1992.

- Zhou, Q., Mathews, J. D., and Tepley, C. A.: A proposed temperature dependent mechanism for the formation of sporadic sodium layers, J. Atmos. Terr. Phys., 55, 513-521, 1993.